nature chemistry

ARTICLES

PUBLISHED ONLINE: 4 JULY 2010 | DOI: 10.1038/NCHEM.702

Experimental probing of conical intersection dynamics in the photodissociation of thioanisole

Jeong Sik Lim and Sang Kyu Kim*

Chemical reactions that occur in the ground electronic state are described well by invoking the Born–Oppenheimer approximation, which allows their development to be rationalized by nuclear rearrangements that smoothly traverse an adiabatic potential energy surface. The situation is different, however, for reactions in electronically excited states, where non-adiabatic transitions occur between adiabatic surfaces. The conical intersection, in which two adiabatic surfaces touch, is accepted widely as the dynamic funnel for efficient non-adiabatic transitions, but its direct experimental probing is rare. Here, we investigate the photodissociation of thioanisole and observe a striking dependence of the relative yields of two reaction channels on the photoexcitation energy as indicated by a dynamic resonance in the product branching ratio. This results from the interference of two different adiabatic states that are in close proximity in the region of a conical intersection. The location of the observed resonance on the multidimensional potential energy surface thus reveals the nuclear configuration of the conical intersection and its dynamic role in the non-adiabatic transition.

Chemical reactions consist of sequences of chemical bond formation and dissociation. Chemical bonds are electrostatic in nature and electrons in motion can make or break bonds between various atoms. In the Born–Oppenheimer approximation, the electronic and nuclear wave functions are separable because of their distinct time scales of motion, which form the premise for the adiabatic description of chemical reactions[1]. In adiabatic processes, the reactants progress to products through transition states that can be described as nuclear rearrangements accompanied by fast electronic motions. Electronic energies calculated for various nuclear configurations thus generate multidimensional potential energy surfaces on which the chemical reaction is driven by forces according to the overall shape of the potential energy surfaces. This model has been extremely successful in describing chemical reactions in the ground electronic states.

For chemical reactions that occur in electronically excited states, however, non-adiabatic transitions in which the nuclear motion induces coupling between two close-lying adiabatic surfaces are not only ubiquitous, but also essential in a number of chemical and biological processes. In particular, the conical intersection, in which two adiabatic surfaces cross in at least the two-dimensional coordinate, is accepted widely as the dynamic funnel for such non-adiabatic transitions[2–5]. Photoisomerization in visional processes[6,7], ultrafast non-radiative decay of excited DNA bases[8–10] and photocatalytic organic reactions[11] are prototypical examples in which non-adiabatic transitions through single or multiple conical intersections play key roles. Accordingly, over the past few decades numerous theoretical and experimental studies investigated the spectroscopic and dynamic role of conical intersections in various chemical processes, such as bimolecular reactions[12], non-radiative energy dephasing[8–10,13], vibronic coupling (including Jahn–Teller)[14] and photodissociation reactions[9,15–25]. In most experimental studies to date, however, the conical intersection region has not been accessed directly by optical excitation, because in polyatomic molecules this region is generally located far from the equilibrium configuration of the ground state in complicated multidimensional nuclear coordinates, although vibration-mediated photodissociation studies have helped to better understand conical intersections[20,21]. This resulted in the structure and dynamics of molecules in the vicinity of the conical intersection being predicted by high-level *ab initio* calculations to aid the interpretation of experimental data[2,3,7,25,26].

In this work, we investigated the photodissociation of thioanisole ($C_6H_5SCH_3$) in the gas phase. The photodissociation reaction proceeds through the dissociation of the sulfur–carbon bond that tethers a methyl group to the molecule. Understanding the reaction first requires us to identify the S_1 vibronic states of thioanisole, which is achieved using the resonant-enhanced two-photon ionization (R2PI) technique. Then we monitored the yield of the $\bullet CH_3$ fragment produced on dissociation as a function of the photoexcitation energy to give the photofragment excitation (PHOFEX) spectrum. We also determined the spatial anisotropy and translational energy distribution of the nascent $\bullet CH_3$ fragment by using the velocity-map ion imaging method.

These experimental techniques allowed us to probe the conical intersection region directly, and resulted in the observation of a dynamic resonance in the photodissociation reaction of thioanisole. At the nuclear configuration in the vicinity of the conical intersection, where the first and second electronically excited states are in close proximity, a coherent superposition of bound (S_1) and repulsive (S_2) electronic states was prepared to give the dynamic resonance in the product branching ratio. Here, the dynamic resonance represents the energetic point at which the relative yields of two different reaction channels change dramatically. The role of the conical intersection in the bond-dissociation dynamics is revealed in the detailed properties of the final products.

Results and discussion

The states and interactions involved in the dissociation reaction are illustrated in Fig. 1. The S–CH_3 bond dissociation from the first electronically excited state of thioanisole (S_1) gives rise to $C_6H_5S\bullet(\tilde{A})$ or $C_6H_5S\bullet(\tilde{X})$, which represent the first excited and ground electronic states of the phenylthiyl radical, respectively. As reported in recent studies of thiophenol dissociation dynamics[15–18], the singly occupied molecular orbital (SOMO) of the $C_6H_5S\bullet(\tilde{A})$ or $C_6H_5S\bullet(\tilde{X})$ radical is localized on sulfur and aligned parallel or

Department of Chemistry and KI for Nano-Century, KAIST, Daejeon 305-701, Korea. *e-mail: sangkyukim@kaist.ac.kr

© 2010 Macmillan Publishers Limited. All rights reserved.

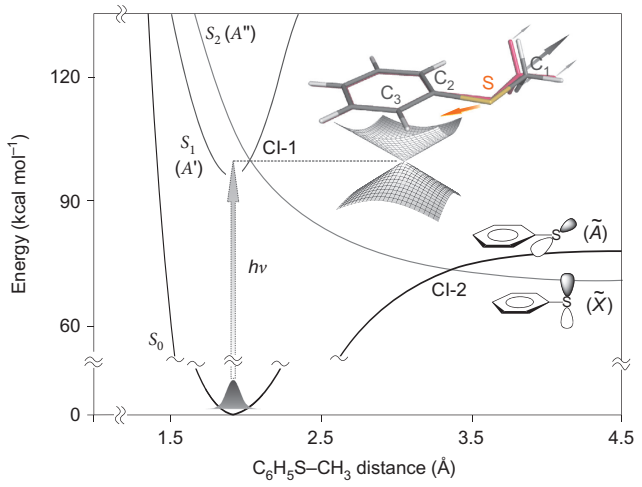

Figure 1 | The three lowest diabatic potential energy curves of thioanisole along the S–CH_3 bond elongation coordinate. A photon induces the optical transition from the ground (S_0) to the first electronically excited state (S_1). S_1 is bound, whereas the upper S_2 state is repulsive along the S–CH_3 elongation coordinate. The S_1 and S_2 states are symmetric (A') or antisymmetric (A'') with respect to the molecular plane. At the asymptotic limit, the S_2 state is diabatically correlated to $C_6H_5S\bullet$ ($\tilde{X}$), whereas S_0 is correlated to $C_6H_5S\bullet$ ($\tilde{A}$). The conical intersections between S_1 and S_2 (CI-1) and S_2 and S_0 (CI-2) are generated at the planar geometry. The simplified SOMO configurations are depicted for the ground ($\tilde{X}$) and excited ($\tilde{A}$) states of the phenylthiyl radical. The calculated nuclear configuration at CI-1 is shown in comparison with the S_1 equilibrium geometry (magenta). The normal mode displacement vector of the 722 cm^{-1} band may represent the reaction coordinate along which the conical intersection is encountered. The branching plane is generated by the two-dimensional nuclear coordinate, the symmetric (in-plane) reaction coordinate and the asymmetric coupling mode (out-of-plane). The conical intersection is on the ($N^{int}-2$)-dimensional seam, where N^{int} is the number of the internal degrees of freedom.

perpendicular to the molecular plane, respectively, with an energy gap of ~8.0 kcal mol^{-1} (refs 16,18).

Similar to the case of thiophenol, S_1 ($\pi\pi^*$) is bound, whereas S_2 with $n\sigma^*$ character is repulsive along the S–CH_3 bond-elongation coordinate. Here, π and π^* are the bonding and antibonding orbitals localized on the benzene moiety, whereas n is the non-bonding orbital localized on sulfur and σ^* is the antibonding orbital along the S–CH_3 bond axis. The S_1 and S_2 states belong to A' and A'', respectively, that is S_1 and S_2 electronic wave functions are symmetric (A') or antisymmetric (A''), respectively, relative to the molecular plane. Therefore, the first conical intersection (CI-1) is expected to be located at the nuclear configuration where the S–CH_3 bond is somewhat elongated at the planar geometry, as shown in Fig. 1. At the asymptotic limit, the S_2 state is diabatically correlated to $C_6H_5S\bullet$ ($\tilde{X}$), whereas S_0 is correlated to $C_6H_5S\bullet$ ($\tilde{A}$). Therefore, the S_2/S_0 conical intersection (CI-2) should play a key role in the bifurcation of the reactive flux into two distinct channels, which leads to $C_6H_5S\bullet$ ($\tilde{A}$) + $\bullet CH_3$ or $C_6H_5S\bullet$ ($\tilde{X}$) + $\bullet CH_3$ products.

Observation of the dynamic resonance in the product branching ratio. Here, we describe the experimentally observed resonance in the product branching ratio between two distinct channels that lead to either $C_6H_5S\bullet$ ($\tilde{A}$) + $\bullet CH_3$ or $C_6H_5S\bullet$ ($\tilde{X}$) + $\bullet CH_3$. We employed R2PI, PHOFEX and velocity-map ion imaging methods to identify the S_1 vibronic states, measure the product yield as a function of the photoexcitation energy and determine the translational energy distributions of products from various excited states of thioanisole, respectively. The R2PI spectrum of the jet-cooled thioanisole shows a number of well-resolved S_1 vibronic bands (Fig. 2)[27], whereas the PHOFEX spectrum obtained by monitoring the $\bullet CH_3$ ($v = 0$) yield as a function of the excitation energy represents the S–CH_3 bond dissociation partial cross–section. The R2PI and PHOFEX spectra showed almost identical patterns until the excitation energy reached the S_1 internal energy region between of 700 and 800 cm^{-1}. Above this energy region, the R2PI signal intensity decreased, whereas the PHOFEX signal persisted with an emerging broad background. These results may indicate that the lifetime of the S_1 state shortens as the pump energy increases with respect to the ~5 ns time window for the ionization detection of the parent molecule.

The speed and spatial distributions of $\bullet CH_3$ ($v = 0$) were determined using the velocity-map ion imaging method[28]. The total translational energy distributions, deduced from the reconstructed three-dimensional ion images, for several excitation energies are shown in Fig. 3. The upper limit for the S–CH_3 bond energy (D_0) of thioanisole is estimated to be 70.8 ± 1.0 kcal mol^{-1} from the maximum total kinetic energy of fragments (E_T) using the relationship $D_0 \leq (h\nu_{ext} - E_T)$ (Fig. 3). This is consistent with the previously reported thermochemical value of 69.4 ± 2.0 kcal mol^{-1} (ref. 29). The distribution from the S_1 origin shows one major Gaussian-shaped peak with a small shoulder in the higher kinetic energy region. From consideration of the energetics, it is obvious that the major peak at $E_t \approx 15.6$ kcal mol^{-1} is caused by the $C_6H_5S\bullet$ ($\tilde{A}$) + $\bullet CH_3$ ($v = 0$) channel, whereas a small shoulder at ~25 kcal mol^{-1} represents the $C_6H_5S\bullet$ ($\tilde{X}$) + $\bullet CH_3$ ($v = 0$) channel. Analysis of the experiment yields an $\tilde{X}/\tilde{A}$ branching ratio of ~0.053, which reveals that $C_6H_5S\bullet$ ($\tilde{A}$) is the dominant product.

A similar pattern indicating $C_6H_5S\bullet$ ($\tilde{A}$) as the major product continued until the excitation energy reached a weakly observed band at 722 cm^{-1}. At this particular vibronic band we found a dramatic increase in the $\tilde{X}/\tilde{A}$ branching ratio (Fig. 2), which gave a sharp resonance. In addition, a sharp resonance was found in the anisotropy parameter. The anisotropy parameter (β) of dissociation, when the reaction time is faster than the rotational period of the parent molecule, represents the vector property of the transition dipole moment with respect to the bond-dissociation axis. The β value varied with the translational energy (Fig. 3), which indicates that the S–CH_3 bond dissociation of thioanisole cannot be described simply by a one-dimensional bond rupture. Other degrees of freedom, such as the C–C–S–C torsional motion during fragmentation, should affect the direction of the final fragments with respect to the transition dipole moment. The effective β value at the maximum translational energy of fragments (β_{eff}) thus more appropriately reflects the orientation of the transition dipole moment with respect to the dissociating chemical bond axis, because the excitation in internal degrees of freedom other than the translational motion along the S–CH_3 elongation coordinate will be lowest for fragments with high translational energies. Notably, the absolute value of the anisotropy parameter reported here is quantitatively less meaningful because of several experimental uncertainties, which include the contribution of the broad background from two-photon excitation. It was found that β_{eff} measured at $E_T = 29$ kcal mol^{-1} showed a resonance feature with a peak value of about -0.7 at 722 cm^{-1} (Fig. 3). The large variation of β_{eff} with excitation energy may indicate that different electronic transitions are mixed at the resonance position. That the S_2–S_0 (n–σ^*) transition dipole moment is perpendicular to the dissociating S–CH_3 bond axis suggests that the transition at 722 cm^{-1} comprises characteristics of both S_1 and S_2. The striking resonance of the product branching ratio observed here provides both energetic and structural information about the dynamic critical point on multi-dimensional potential energy surfaces, as each vibronic band in the R2PI spectrum represents its own nuclear configuration in multidimensional coordinates.

© 2010 Macmillan Publishers Limited. All rights reserved.

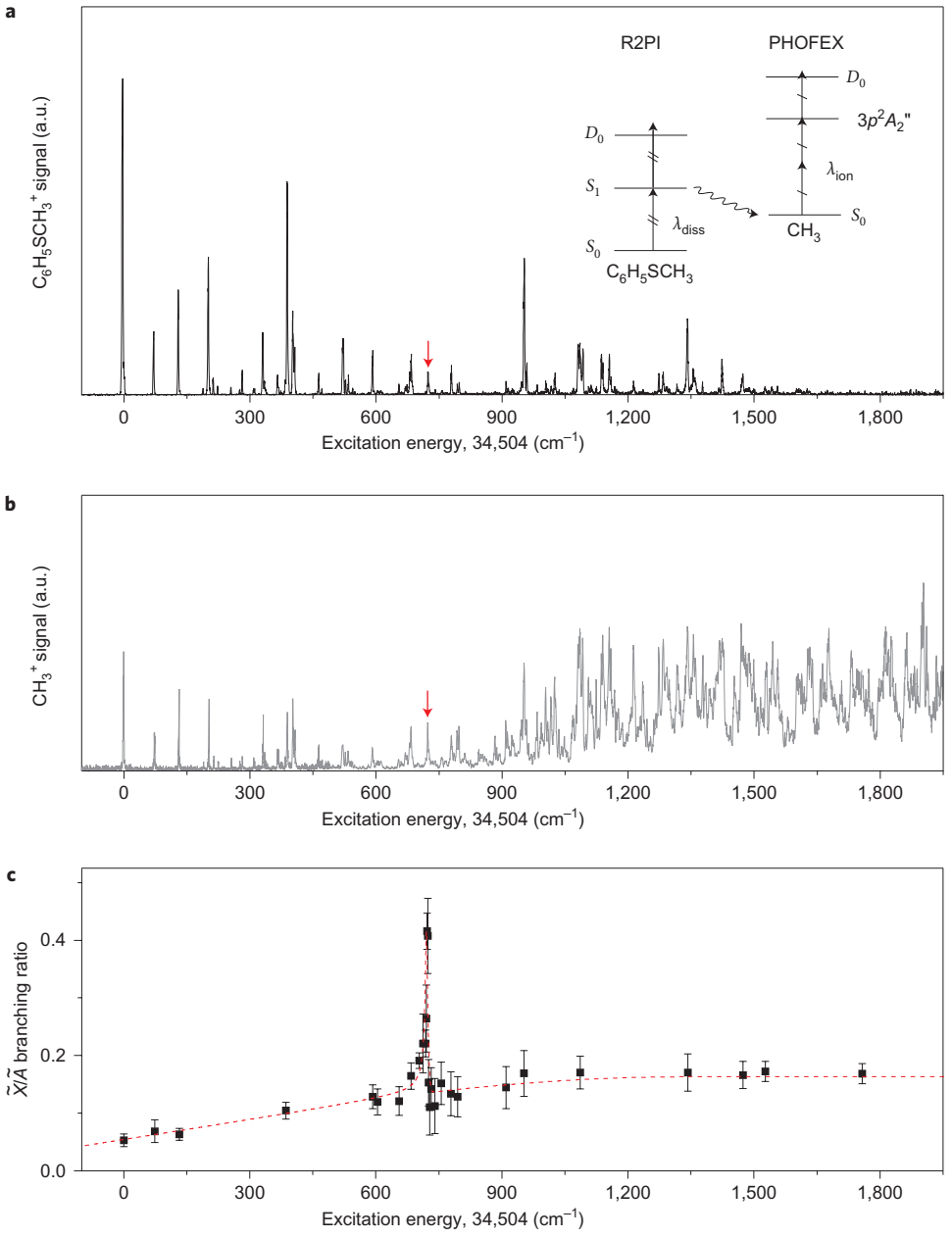

Figure 2 | The S_1 vibronic levels, the total $\bullet CH_3$ ($v = 0$) fragment yield and the $\tilde{X}/\tilde{A}$ branching ratio plotted as a function of the photoexcitation energy. **a**, R2PI spectrum of jet-cooled thioanisole. Thioanisole adopts a planar geometry in the ground state[27], which is maintained in S_1 (Supplementary Fig. S1). **b**, PHOFEX spectrum to monitor $\bullet CH_3$ ($v = 0$) versus pump energy. The nascent $\bullet CH_3$ fragment ($v = 0$) was probed by (2 + 1) ionization with a laser pulse ($\Delta t \approx 5$ ns) at 333.45 nm using the *Q* transition via $3p^2A_2''$ without rotational selection (Supplementary Fig. S2). **c**, The $\tilde{X}/\tilde{A}$ branching ratio shows a sharp resonance feature at an internal energy of 722 cm^{-1}. All the peak positions at which the product branching ratios were measured precisely are listed in the Supplementary Information. The dotted line is a visual aid to show the asymmetric shape of the branching ratio. a.u. = arbitrary units.

Nature of the resonance band and non-adiabatic dynamics at the conical intersection. We describe here the method used to interpret the striking resonance feature in the product branching ratio. To characterize the 722 cm^{-1} band of S_1, we used two-photon two-colour (1 + 1′) mass-analysed threshold ionization (MATI) spectroscopy, in which the first photon was fixed at the specific S_1–S_0 transition and the second photon was varied to identify the vibrational state of the thioanisole cation (D_0) in a pulsed-field ionization condition. In the MATI spectrum taken with the 722 cm^{-1} band of S_1 as an intermediate state, according to the propensity rule ($\Delta v = 0$) in the D_0–S_1 ionization process, the band of the same normal mode as the intermediate state was enhanced strongly (Supplementary Fig. S4) to give the associated D_0 vibrational frequency of 743 cm^{-1}. This closely matches the theoretical value of 733 cm^{-1} for the 7a vibrational mode of the thioanisole cation that corresponds to the C_1–S–C_2 asymmetric stretching motion (Supplementary Table S2). Therefore, the 722 cm^{-1} band is ascribed to the C_1–S–C_2 asymmetric stretching mode. The *ab initio* calculation using CASSCF with a basis set of 6-31G** (see Supplementary Information) revealed that the molecular structure at CI-1 consisted of a significantly elongated S–CH_3 bond and a shortened C_2–S bond compared with the S_0 structure (Table 1), which corresponds well with the molecular structure at the classical turning point of the 722 cm^{-1} band. Therefore, nuclear displacement associated with the 722 cm^{-1}

© 2010 Macmillan Publishers Limited. All rights reserved.

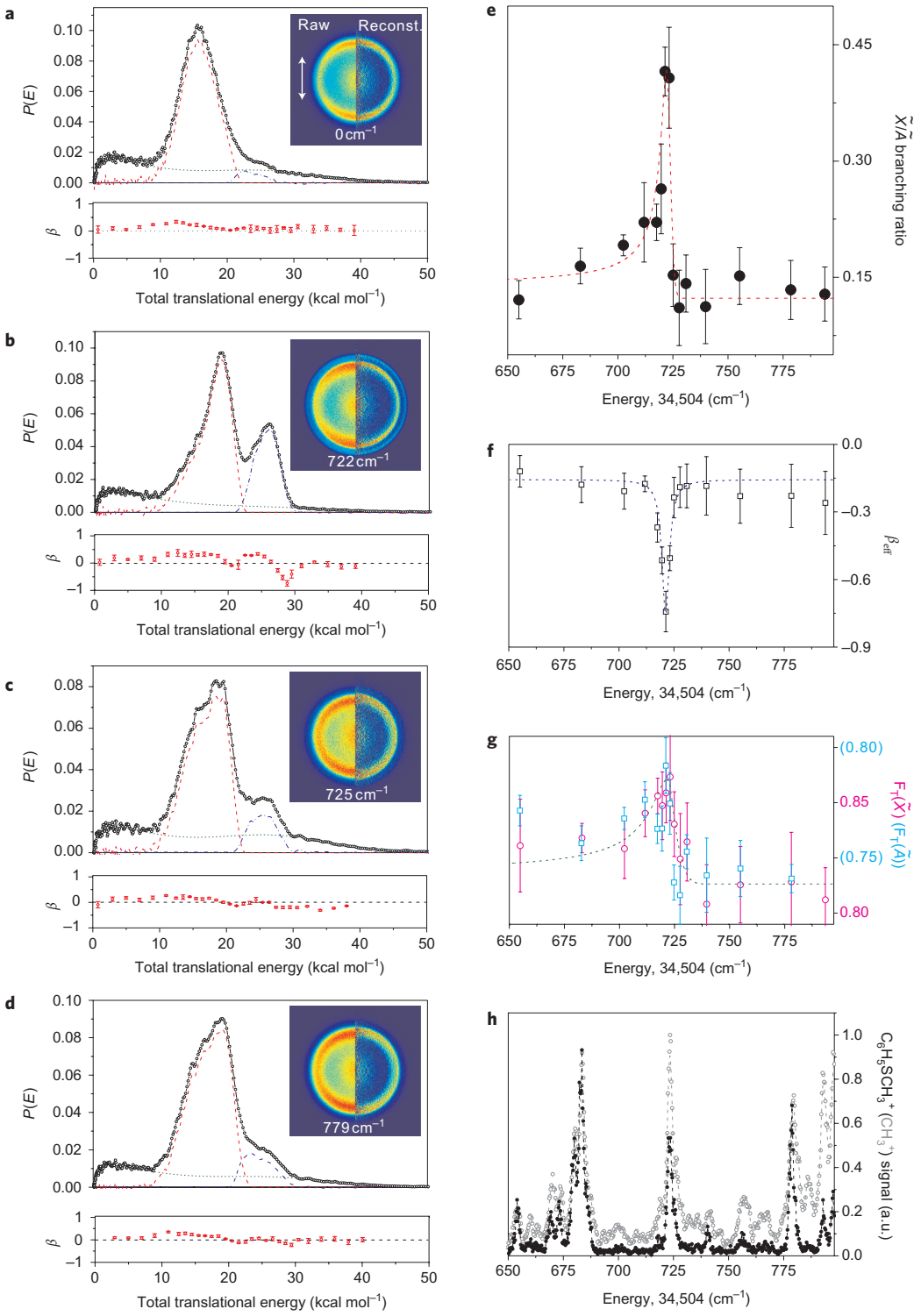

Figure 3 | Dynamic observables of products from the excited thioanisole near the conical intersection region. a–d, Total translational energy distributions ($P(E)$) deduced from CH_3^+ ($v = 0$) images at the excitation energies of (**a**) 34,504 cm^{-1}, (**b**) 35,226 cm^{-1}, (**c**) 35,229 cm^{-1} and (**d**) 35,282 cm^{-1}. Corresponding S_1 internal energies are given in the insets, with the raw image on the left and the reconstructed image on the right. The ion image probing $\bullet CH_3$ ($v_2 = 1$) shows an identical pattern to that of $\bullet CH_3$ ($v = 0$) (Supplementary Fig. S3). The anisotropy parameter (β) is deduced from $I(\theta) \propto 1 + \beta(E)P_2(\cos\theta)$, where θ is the angle between the pump polarization and recoil vector and $P_2(\theta)$ is the second-order Legendre polynomial. The broad background shows the quadratic dependence on the pump laser intensity. Deconvolution of the total translational distribution into three components is shown as dotted lines below the experimental results. For the contribution of the broad background, the low-energy part was assumed to be smoothly connected to the high-energy part. The energy gap between $\tilde{A}$ and $\tilde{X}$ was fixed at 8.0 kcal mol^{-1} for further deconvolution into components of the $\tilde{A}$ and $\tilde{X}$ channels. Polarizations of the pump and probe are denoted by the arrow in (**a**) (inset). **e**, The $\tilde{X}/\tilde{A}$ branching ratio versus the S_1 internal energy. A dotted line is drawn as a visual aid. **f**, β_{eff} at the translational energy of 29 kcal mol^{-1} versus the internal energy. **g**, Translational energy partitioning ratios (E_{trans}/E_{avl}) for $\tilde{A}$ ($F_T(\tilde{A})$) (blue circles) and $\tilde{X}$ ($F_T(\tilde{X})$) (red circles) channels, where $E_{avl} = h\nu - D_0$. **h**, R2PI (filled circles) and PHOFEX (open circles) spectra in the corresponding energy region. a.u. = arbitrary units.

© 2010 Macmillan Publishers Limited. All rights reserved.

Table 1 | Calculated significant structural features of thioanisole.

	S_0	S_1	S_1*	CI-1
S-C_1 (Å)	1.860	1.863	1.993	2.062
S-C_2 (Å)	1.813	1.786	1.780	1.756
C_2-S-C_1 (°)	102.9	103.7	99.9	103.0
C_3-C_2-S (°)	116.1	115.3	113.2	110.4

Values are given for the S_0 ground state, the zero-point level of S_1, the classical turning point of the 722 cm^{-1} band (S_1^*) and CI-1. Full details are given in Supplementary Table S3.

band most likely allows for the direct transition from S_0 to the S_1/S_2 superposition state in the vicinity of the conical intersection. The broad background signal in PHOFEX (Fig. 2) above the dynamic resonance band should result from the coupling of optically bright S_1 to dark S_2 states, consistent with the characteristic of the 722 cm^{-1} band as a mediator for the direct probing of the conical intersection region in terms of energetics and nuclear configuration.

At the dynamic resonance band at 722 cm^{-1}, the reactive flux of the S_2 character prepared directly in the vicinity of CI-1 gives less vibrational and thus larger translational energies for departing fragments compared to those of the S_1 component. This is because the former undergoes prompt bond rupture on the repulsive surface, whereas the latter resides in the bound potential with some recurrences, which include the eventual intramolecular vibrational redistribution process coupled to S_2 for dissociation. Therefore, a higher non-adiabatic transition probability at CI-2 that leads to $C_6H_5S\bullet(\tilde{X})$ is expected for fragments with a higher relative translational energy, as predicted by the Landau–Zener formula[30]. This is consistent with our experimental finding that the $\tilde{X}/\tilde{A}$ branching ratio and the translational partitioning ratio correlate well in the resonance region (Fig. 3). Specifically, the translational energy distributions associated with the $\tilde{X}$ and $\tilde{A}$ channel suddenly shift to the high-energy region and then return to the original region as the excitation energy passes through the narrow energy range near the 722 cm^{-1} band. The dynamic resonance feature in the $\tilde{X}/\tilde{A}$ branching ratio shows an asymmetric shape, which may result from the interference of two reactive fluxes of S_1 and S_2 character. As the relative phase of the S_1 and S_2 components varies over the narrow CI-1 energy range, it is possible that the Fano-type asymmetric nature of the resonance is manifested in the product branching ratio[31]. An ordinary S_1/S_2 vibronic coupling mechanism does not seem a suitable explanation of these dynamic features of quantum-mechanical interferences. Therefore, the dynamic resonance in the product branching ratio observed here may represent the coherently excited S_1/S_2 superposition state, which is accessible only in the vicinity of CI-1, where two multidimensional potential energy surfaces are in close proximity (Fig. 1). The weak intensity of the dynamic resonance band at 722 cm^{-1} (Fig. 2) indicates that the nuclear configuration spanned by the corresponding normal mode is quite far from the S_0/S_1 equilibrium structures, as shown by the experimental fact that the origin band is absent in the $(1+1')$ MATI spectrum through the 722 cm^{-1} band, whereas the $0–0^+$ origin band is observed most strongly in the MATI spectrum through the $S_1–S_0$ origin band (Supplementary Fig. S4). Accordingly, the vertical excitation energy for the bound-to-repulsive $S_2–S_0$ transition is expected to lie well above CI-1, which is located far from the equilibrium structure. In the $S_1–S_0$ transition, because of the resonance features of the bound S_1 states, the CI-1 region could be reached optically in terms of both nuclear configuration and energetics. This is consistent with the experimental observation that only the product branching ratio peaks strikingly at the CI-1 region, whereas the total fragmentation yield and absorption cross-section show no drastic change.

That $C_6H_5S\bullet(\tilde{A})$ is the major product at photoexcitation energies above the dynamic resonance position indicates that the reactive flux on S_2, if prepared indirectly through vibronic coupling through the optically active S_1 state, prefers to follow the adiabatic path at CI-2. The vibrational excitation involved in the coupling of the optically active S_1 to dark S_2 states may be responsible for this observation. In the vibronic coupling process, the optically active a' vibrational mode in S_1 (A') should be coupled to optically dark a'' modes of S_2 (A''). This symmetry-conservation requirement induces vibrational excitation along the out-of-plane mode, which may act as the asymmetric coupling mode in the branching plane for CI-2. In some sense, this is also equivalent to the geometric phase effect for the encircled reaction path around the conical intersection, because two reactive fluxes bifurcated at the conical intersection with different phases interfere with one another in the exit channel, which leads to the different symmetry of the nuclear wave function[24]. The spread of the reactive flux along the asymmetric coupling mode diminishes the non-adiabatic transition probability, to give the smaller $\tilde{X}/\tilde{A}$ branching ratio, because the non-adiabatic transition probability decreases for the reactive flux on the potential energy surface region, where the vertical energy gap between two adiabats is large as a result of the excitation along the asymmetric coupling mode. Quantum states above CI-1, after some recurrences in S_1, may undergo intramolecular vibrational redistribution to be trapped in the upper adiabat before the non-adiabatic leakage through CI-1, which results in internal conversion or chemical bond-breaking processes. Our experimental characterization of the CI-1 region provides the nuclear configuration near the dynamic funnel for such non-adiabatic transitions.

Conclusions

In conclusion, we used one-photon optical excitation to probe the critical nuclear configuration near the conical intersection directly. The dynamic role of the conical intersection manifests as a sharp resonance in the product branching ratio between the $C_6H_5S\bullet(\tilde{A})+\bullet CH_3$ $(v=0)$ and $C_6H_5S\bullet(\tilde{X})+\bullet CH_3$ $(v=0)$ channels. The asymmetric shape of the dynamic resonance may indicate that a coherent superposition of the S_1 (bound) and S_2 (continuum) states occurred in the vicinity of the conical intersection. The resonance in the product branching ratio is accompanied by a resonance in the translational energy partitioning ratio, which gives a qualitative but reasonable explanation for non-adiabatic dynamics at CI-2.

The dynamic role of the conical intersection in the photodissociation reaction turns out to be quite remarkable and could be used for reaction control in terms of both product branching ratio and energy partitioning, which can be extended further to stereochemistry. To search for other possible critical points on the multidimensional conical intersection seam in this or similar systems may be intriguing, but certainly high-level theoretical calculations are desirable. Investigating the state near the conical intersection using a strong external field or coherent phase control with two different optical excitation schemes would also be interesting in order to explore further the reaction dynamics at the edge of the conical intersection, the most critical point in the chemical reaction.

Methods

To obtain the R2PI and PHOEX data, an excitation laser pulse ($\Delta t \approx 5$ ns, $\Delta\bar{\nu} \approx 0.07$ cm^{-1}) was continuously scanned while monitoring the parent ion or the nascent $\bullet CH_3$ radical ion signals, respectively. For the velocity-map ion imaging set-up, detailed experimental conditions are described elsewhere[16]. Briefly, the sample was heated to 35 °C, mixed with a helium carrier gas and expanded into a vacuum through a 0.5 mm diameter nozzle orifice with a backing pressure of ~3 atmospheres. The $\bullet CH_3$ images were taken for all velocity components and averaged over 80,000–720,000 laser shots. The three-dimensional images were reconstructed from raw images using the BASEX algorithm. Total translational energy distributions were corrected by the Jacobian factor. For $(1+1')$ MATI spectroscopy, the long-lived high-n,l Rydberg states that converge to the cationic ground vibrational levels of thioanisole were generated before they were ionized by the

© 2010 Macmillan Publishers Limited. All rights reserved.

pulsed electric field ($\Delta t \approx 5$ μs; ~160 V cm^{-1}). The detailed experimental set-up for the MATI spectroscopy was described previously[32].

Received 27 October 2009; accepted 13 May 2010; published online 4 July 2010

References

1. Born, M. & Oppenheimer, R. On the quantum theory of molecules. *Ann. Phys.* **84,** 457–484 (1927).
2. Yarkony, D. R. Diabolical conical intersections. *Rev. Mod. Phys.* **68,** 985–1013 (1996).
3. Domcke, W., Yarkony, D. R. & Köppel, H. *Conical Intersections: Electronic Structure, Dynamics and Spectroscopy* (World Scientific, 2004).
4. Worth, G. A. & Cederbaum, L. S. Beyond Born–Oppenheimer: molecular dynamics through a conical intersection. *Annu. Rev. Phys. Chem.* **55,** 127–158 (2004).
5. Köppel, H., Domcke, W. & Cederbaum, L. S. Multimode molecular dynamics beyond the Born–Oppenheimer approximation. *Adv. Chem. Phys.* **57,** 59–246 (1984).
6. Kohler, B. E. Octatetraene photoisomerization. *Chem. Rev.* **93,** 41–54 (1993).
7. Garavelli, M. *et al.* The $C_5H_6NH_2^+$ protonated Shiff base: an *ab initio* minimal model for retinal photoisomerization. *J. Am. Chem. Soc.* **119,** 6891–6901 (1997).
8. Kang, H. *et al.* Intrinsic lifetime of the excited state of DNA and RNA bases. *J. Am. Chem. Soc.* **124,** 12958–12959 (2002).
9. Soboleski, A. L., Domcke, W., Dedonder-Lardeux, C. & Jouvet, C. Excited-state hydrogen detachment and hydrogen transfer driven by repulsive $^1\pi\sigma^*$ states: a new paradigm for nonradiative decay in aromatic biomolecules. *Phys. Chem. Chem. Phys.* **4,** 1093–1100 (2002).
10. Perun, S., Sobolewski, A. L. & Domcke, W. Conical intersections in thymine. *J. Phys. Chem. A* **110,** 13238–13244 (2006).
11. Trushin, S. A., Fuß, W. & Schmid, W. E. Conical intersections, pseudorotation and coherent oscillations in ultrafast photodissociation of group-6 metal hexacarbonyls. *Chem. Phys.* **259,** 313–330 (2000).
12. Schnieder, L. *et al.* Experimental studies and theoretical predictions for the $H+D_2 \rightarrow HD+D$ reaction. *Science* **269,** 207–210 (1995).
13. Raab, A., Worth, G. A., Meyer, H.-D. & Cederbaum, L. S. Molecular dynamics of pyrazine after excitation to the S_2 electronic state using a realistic 24-mode model Hamiltonian. *J. Chem. Phys.* **110,** 936–946 (1999).
14. Bersuker, I. B. *The Jahn–Teller Effect and Vibronic Interactions in Modern Chemistry* (Springer, 1984).
15. Lim, J. S. , *et al.* Intramolecular orbital alignment observed in the photodissociation of [D1]thiophenol. *Angew. Chem. Int. Ed.* **45,** 6290–6293 (2006).
16. Lim, I. S., Lim, J. S., Lee, Y. S. & Kim, S. K. Experimental and theoretical study of the photodissociation reaction of thiophenol at 243 nm: intramolecular orbital alignment of the phenylthiyl radical. *J. Chem. Phys.* **126,** 034306 (2007).
17. Lim, J. S., Lee, Y. S. & Kim, S. K. Control of intramolecular orbital alignment in the photodissociation of thiophenol: conformational manipulation by chemical substitution. *Angew. Chem. Int. Ed.* **47,** 1853–1856 (2008).
18. Devine, A. L., Nix, M. G. D., Dixon, R. N. & Ashfold, M. N. R. Near-ultraviolet photodissociation of thiophenol. *J. Phys. Chem. A* **112,** 9563–9574 (2008).
19. Ashfold, M. N. R. *et al.* The role of $\pi\sigma^*$ excited state in the photodissociation of heteroaromatic molecules. *Science* **312,** 1637–1640 (2006).
20. Crim, F. F. Vibrationally mediated photodissociation: exploring excited-state surfaces and controlling decomposition pathways. *Annu. Rev. Phys. Chem.* **44,** 397–428 (1993).
21. Hause, M. L., Yoon, Y. H., Case, A. S. & Crim, F. F. Dynamics at conical intersections: the influence of O–H stretching vibrations on the photodissociation of phenol. *J. Chem. Phys.* **128,** 104307 (2008).
22. Butler, L. J. Chemical reaction dynamics beyond the Born–Oppenheimer approximation. *Annu. Rev. Phys. Chem.* **49,** 125–171 (1998).
23. Keller, J. S., Kash, P. W., Jensen, E. & Butler, L. J. Selective bond fission in methyl mercaptan at 193 nm via radial derivative coupling between the 2 ^1A and 1 ^1A adiabatic electronic states. *J. Chem. Phys.* **96,** 4324–4329 (1992).
24. Abe, M. *et al.* Geometric phase effects in the coherent control of the branching ratio of photodissociation products of phenol. *J. Chem. Phys.* **124,** 224316 (2006).
25. Vieuxmaire, O. P. J., Lan, Z., Sobolewski, A. L. & Domcke, W. *Ab initio* characterization of the conical intersections involved in the photochemistry of phenol. *J. Chem. Phys.* **129,** 224307 (2008).
26. Lee, A. M. D. *et al.* Substitution effects on dynamics at conical intersections: α,β-enones. *J. Phys. Chem. A* **111,** 11948–11960 (2007).
27. Vondrak, T., Sato, S., Spirko, V. & Kimura, K. Zero kinetic energy (ZEKE) photoelectron spectroscopic study of thioanisole and its van der Waals complexes with argon. *J. Phys. Chem. A* **101,** 8631–8638 (1997).
28. Eppink, A. T. J. B. & Parker, D. H. Energy partitioning following photodissociation of methyl iodide in the A band: a velocity mapping study. *J. Chem. Phys.* **110,** 832–844 (1999).
29. McMillen, D. F. & Golden, D. M. Hydrocarbon bond dissociation energies. *Ann. Rev. Phys. Chem.* **33,** 493–532 (1982).
30. Zener, C. Non-adiabatic crossing of energy level. *Proc. R. Soc. Lond. A* **137,** 696–702 (1932).
31. Fano, U. Effects of configuration interaction on intensities and phase shifts. *Phys. Rev.* **124,** 1866–1878 (1960).
32. Beak, S. J., Choi, K.-W., Choi, Y. S. & Kim, S. K. Resonant-enhanced two photon ionization and mass-analyzed threshold ionization spectroscopy of jet-cooled 2-aminopyridines (2AP–NH_2, –NHD, –NDH, –ND_2). *J. Chem. Phys.* **117,** 2131–2140 (2002).

Acknowledgements

We thank Y.S. Lee and H. Choi for discussions, and assistance from J. Yoon and S. Han is appreciated. This work was supported by the National Research Foundation of Korea (2010-0001635, –0000068, –0015031; 313-2008-2-C00401) and KAIST (high-risk high-return).

Author contributions

J.S.L. and S.K.K. conceived and designed the experiments, J.S. Lim performed the experiments, J.S. Lim and S.K. Kim analysed and interpreted data, and J.S. Lim and S.K. Kim co-wrote the paper.

Additional information

The authors declare no competing financial interests. Supplementary information accompanies this paper at www.nature.com/naturechemistry. Reprints and permission information is available online at http://npg.nature.com/reprintsandpermissions/. Correspondence and requests for materials should be addressed to S.K.K.

© 2010 Macmillan Publishers Limited. All rights reserved.